AIAA 2003-3766

Estimates Of The Orbiter RSI Thermal Protection System Thermal Reliability

P. Kolodziej and D.J. Rasky
NASA Ames Research Center
Moffett Field, CA 94035

36th AIAA Thermophysics Conference
23-26 June 2003
Orlando, Florida

ESTIMATES OF THE ORBITER RSI THERMAL PROTECTION SYSTEM THERMAL RELIABILITY

P. Kolodziej* and D.J. Rasky†
NASA Ames Research Center
Moffett Field, CA 94035

Abstract

In support of the Space Shuttle Orbiter post-flight inspection, structure temperatures are recorded at selected positions on the windward, leeward, starboard and port surfaces. Statistical analysis of this flight data and a non-dimensional load interference (NDLI) method are used to estimate the thermal reliability at positions were reusable surface insulation (RSI) is installed. In this analysis, structure temperatures that exceed the design limit define the critical failure mode. At thirty-three positions the RSI thermal reliability is greater than 0.999999 for the missions studied. This is not the overall system level reliability of the thermal protection system installed on an Orbiter. The results from two Orbiters, OV-102 and OV-105, are in good agreement. The original RSI designs on the OV-102 Orbital Maneuvering System pods, which had low reliability, were significantly improved on OV-105. The NDLI method was also used to estimate thermal reliability from an assessment of TPS uncertainties that was completed shortly before the first Orbiter flight. Results from the flight data analysis and the pre-flight assessment agree at several positions near each other. The NDLI method is also effective for optimizing RSI designs to provide uniform thermal reliability on the acreage surface of reusable launch vehicles.

Nomenclature

CDF	normal cumulative distribution function
ETR	eastern test range
FOS	factor of safety (μ_S/μ_L or T_S/T_L)
IOR	index of reliability, see Eq.(2)
MOS	margin of safety ($\mu_S-\mu_L$ or T_S-T_L)
N	number of observations
NA	data not available
NDLI	Non-Dimensional Load Interference
OFT	Orbiter Flight Test
OMS	Orbital Maneuvering System
OV	Orbiter Vehicle
PDF	normal probability density function
p_i	(i-0.5)/N, i = 1 to N
Q	total integrated heat load
r^2	correlation coefficient $(\sigma_{xy}/\sigma_x\sigma_y)^2$
R	reliability
RSI	reusable surface insulation
RSS	root sum squares deviation
T	temperature, K
T_{margin}	structure temperature margin at $+3\sigma$ conditions ($T_D-T_{max,3\sigma}$), K
T_{max}	maximum temperature of structure at nominal conditions, K
$T_{max,3\sigma}$	maximum temperature of structure at $+3\sigma$ conditions, K
WTR	western test range
x	integration variable in Eq.(1)
$Z(p_i)$	p_ith normal distribution percentile
$\Delta T_{m,n}$	temperature deviation
λ_j	uncertainty ratio or variation (μ_j/σ_j)
μ_j	expected mean value, K
σ_j	sample standard deviation, K
σ_{xy}	covariance of x and y
σ_x	sample standard deviation of the independent parameter x
σ_y	sample standard deviation of the dependent parameter y

Subscripts

A	applied load
c	effective thermal capacitance of the substructure
D	design limit
I	initial
i	index of ordered observation
j	L or S
k	thermal conductivity of the TPS material
L	load
m	index of perturbed quantity
n	number of standard deviations
o	observed value
p	predicted value
ref	reference value
q	surface heating rate
S	strength
t	time of boundary layer transition from laminar to turbulent
To	initial temperature of the RSI to substructure inner bondline

*Member AIAA, Research Scientist
†Senior Member AIAA, Senior Staff Scientist

Introduction

In the early 1970s conceptual designs of the Space Shuttle Orbiter thermal protection system (TPS) were based on preliminary measurements of the TPS properties and the aerothermal heating environments.[1,2] To compensate for the large uncertainties in this data the early reusable TPS concepts were designed with additional margin or thickness. Because any additional TPS mass directly subtracted from the Orbiter payload capability, it became very important to carefully optimize the reusable TPS for performance and reliability. With significant testing and analysis, the uncertainties were gradually reduced and the conceptual designs eventually matured into an operational system that was installed on five Orbiters, and has been flown successfully on more than 100 missions. Heating uncertainties for the first Orbiter flight are shown in Fig. 1.[3] The largest uncertainty (15% to 101%) occurs at the shock impingement area on the wing leading edge.

The Orbiter fleet provides a unique opportunity for acquiring data on the performance of TPS designs that have flown on more than one mission. Structure temperatures are recorded at selected positions on the windward, leeward, starboard and port surfaces as part of the Orbiter maintenance program. Because of these repetitive measurements, statistical analysis can be used to determine with high confidence the mean value and standard deviation at each position. Measurements from a single set of flight data, such as that recorded on more typical TPS designs (capsules, planetary entry probes, military warheads), would have lower confidence levels.

During re-entry, the Orbiter experiences a diverse, complex heating environment that presented many challenges in thermal-structural design and required the development of several advanced TPS materials. Reinforced-Carbon-Carbon, a material with the highest temperature capability, is installed on the nose and wing leading edges where the most severe aerothermal heating occurs. Behind these leading edges, where lower heating occurs, reusable surface insulation (RSI) materials are used to protect the airframe structure. Most of the structure temperatures published in the post-flight inspection reports are at positions where RSI is installed.

Because each position has a unique RSI design and a unique heating environment, the flight data provides extensive information over a wide range of designs and conditions. The various designs at each position capture many of the actual uncertainties and randomness affecting the TPS performance including variations in initial temperature, material properties, geometry, structure attachment, gaps and joints. Also captured at each position are uncertainties and randomness affecting the local heating environment including: trajectory and atmospheric variations, turbulent transition, finite rate chemistry, and any unusual flow phenomena.

The purpose of this paper is to present a non-dimensional load interference (NDLI) approach for calculating the thermal reliability of RSI designs from the structure temperature measurements. To demonstrate the practicality of the NDLI approach, it is also used to estimate RSI thermal reliabilities from an early pre-flight analysis of the uncertainties affecting Orbiter TPS performance.

Thermal Reliability Analysis

Following conventional machine design formalism, the NDLI method was developed for estimating thermal reliability.[4] In developing mechanical components with high reliability, it is standard practice to use large factors of safety (>4), with a strength that is several times greater than the load, under circumstances where large uncertainties, randomness and small precision are present. When the materials and load environments are well characterized and controlled, lower factors of safety (<2) may be used to minimize mass and cost. Reliability may be estimated in both scenarios by analysis of the interference between the strength and load distributions.[5] For normal probability distributions of strength and load, reliability is defined by:

$$R = \frac{1}{\sqrt{2\pi}} \int_{-\infty}^{IOR} \exp\left(\frac{-x^2}{2}\right) dx \qquad (1),$$

where the index of reliability (IOR) is given by

$$IOR = \frac{FOS - 1}{\sqrt{FOS^2 \lambda_S^2 + \lambda_L^2}} \qquad (2).$$

Reliability (R) depends on three non-dimensional parameters: factor of safety (FOS), strength uncertainty ratio (λ_S) and load uncertainty ratio (λ_L). The uncertainty ratio is also known as the coefficient of variation. Intrinsic functions for evaluating the integral in Eq. (1) are available in commercial spreadsheet software. In cases where the strength or load is described by other probability distributions, such as the

Weibull distribution, reliability may be calculated by numerical integration.

High reliability is achieved when the mean strength (μ_S) is greater than the mean load (μ_L), and the standard deviations (σ_S,σ_L) cause little interference or overlap. The interference area in Fig. 2, where load exceeds strength and causes failure, may be minimized by either reducing the standard deviations (σ_S,σ_L) or moving the means (μ_S,μ_L) further apart. An upper limit (IOR=∞) of 100% reliability occurs when FOS>1 and λ_L=λ_S=0 because there is no overlap of the distributions. When FOS=1, a 50% reliability occurs for any combination of nonzero uncertainty ratios.

The relationship between the index of reliability (IOR) and reliability (R) is shown in Fig. 3. Often components are designed for a normally distributed load with only a mean value used to define strength (λ_S=0), which simplifies Eq. (2) to:

$$IOR = \frac{\mu_S - \mu_L}{\sigma_L} \qquad (3).$$

Fig. 3 shows that the common 3σ design with μ_S=μ_L+3σ_L and IOR=3 has a reliability of 99.87%. A 1σ design has a reliability of 84.13%. For practical purposes, a reliability of 99.9999% (six 9's) occurs when IOR>4.768.

Fig. 4 shows the relationship between IOR, λ_L, and FOS for a well-characterized material that has a narrow variation in strength (λ_S=0.030), such as the Orbiter RSI. As characterization or control of the load environment improves, and λ_L approaches zero, the reliability increases. Reliability also increases with additional margin or FOS. Increasing the FOS, for example, by increasing the RSI thickness provides additional insulation of the structure and improves its thermal reliability.

Thermal Strength and Load Definitions

Several definitions for thermal strength and load were examined in the development of NDLI (see Ref. 4). Fundamentally, the load refers to the heat load environment (Q_L), and the strength is the relevant heat load capability (Q_S) for that environment. Alternate definitions based on temperature and TPS thickness may be more practical depending on the critical failure mode being addressed by the design approach. For RSI designs, two of the most important critical failure modes are: high surface temperatures that melt or ablate the RSI material, and high structure temperatures that cause failure of the supporting airframe.

When the critical failure mode under analysis is the structure supporting the TPS, the load and strength may be defined by:

$$\begin{aligned} T_L &= T_A - T_I \quad \sim Q_L \\ T_S &= T_D - T_I \quad \sim Q_S \end{aligned} \qquad (4).$$

The load (T_L) is the difference between the maximum observed temperature (T_A) of the structure and its initial temperature (T_I). The strength (T_S) is the difference between the design limit temperature (T_D) of the structure and its initial temperature (T_I). The RSI is adhesively bonded to aluminum or graphite-epoxy structures that have multi-mission design limit temperatures (T_D) of 450 K, except on the Orbital Maneuvering System (OMS) pod where T_D=395 K.[6]

Orbiter Flight Data

The TPS undergoes a thorough inspection after each flight to assess the maintenance required to refurbish it for flight and to monitor its long-term performance. As part of this process, structure temperatures are recorded in flight and published in the post-flight inspection reports at as many as thirty-three positions.[7,8] A preliminary analysis of data from twenty-seven flights of OV-102 and eighteen flights of OV-105 are presented in this paper. Data from the early flights of OV-102 that were not published in the post-flight reports were acquired from the NASA Space Shuttle Vehicle Engineering Office web site.[9] The initial temperature is calculated by subtracting the rise temperature from the peak temperature.

For accurate estimates of reliability using Eq. (1) the strength and load data should be distributed with normal probability. An effective tool to assess the normality of distributions is a quantile-quantile plot. To obtain this plot the temperature data measured at a position are plotted on linear scales, the *i*th-ordered measurement against $Z(p_i)$.[10] Normally distributed data plot as a straight line and have a correlation coefficient (r^2) of one. No correlation exists when r^2=0.

Fig. 5 compares dimensionless OV-102 flight data at position P6 to the normal cumulative distribution function (CDF) for strength and load. The r^2 coefficients from the corresponding quantile-quantile plots are almost one, indicating that the data are almost normally distributed. P6 was selected as a representative example because the r^2 values at P6 for

T_L (0.913) and T_S (0.902) correspond to the median values for all of the OV-102 positions.

The NDLI parameters (λ_L,λ_S,FOS,IOR) listed in Table 1 and 2 are from a statistical analysis of the OV-102 and OV-105 flight data and Eq. (2). The results from Table 1 and 2 are shown in Fig. 6, 7, 8 and 9 at each position to illustrate trends and facilitate comparison. The number of measurements (N) at each position ranges from ten to twenty-seven. This preliminary analysis used all of the available data without adjustments for high and low temperature outliers. At some positions, less than the full set of measurements for OV-102 (N=27) and OV-105 (N=18) were available for analysis, possibly due to instrumentation failure. A higher level of confidence in the estimates of λ_L, λ_S, FOS, and IOR is associated with values of r^2 approaching one and a large number of measurements. For T_S, r^2 ranges from 0.683 to 0.982 (Table 1,2), and r^2 for T_L ranges from 0.622 to 0.983 (Table 1,2). A formal confidence level analysis is beyond the scope of this preliminary analysis.

Results

Two Orbiters, OV-102 and OV-105, were selected for analysis to determine if the NDLI approach provides consistent results. OV-105 was assembled after OV-102 and incorporated more than ten years of operational experience, modifications and improvements. Because all of the Orbiters have nearly identical outer mold lines and re-enter the atmosphere on tightly constrained trajectories, the thermal load environments should be very similar. If the design of the RSI and airframe structure are identical at each position on OV-102 and OV-105 then the local factor of safety and thermal reliability for both vehicles will be very similar. Some improvements in the RSI design on OV-105 may have addressed localized operational problems and may appear as an increase in local thermal reliability.

Mean values of λ_L, λ_S, FOS and IOR for the windward, leeward, starboard and port surfaces are listed in Table 3 and in each figure. Because of the diversity in both the aerothermal heating and the RSI designs, it is useful to examine the trends exhibited on the windward, leeward, starboard and port surfaces. Consistency can be examined by comparing the trends on the starboard and port surfaces, and by comparing the trends on OV-102 and OV-105. Only several of the more important features are discussed in the following sections, due to limited space.

Thermal Load Uncertainty or Variation

At high angle of attack (40°) the leeward surface of a hypersonic vehicle generally experiences larger variations in aerothermal heating than the windward surface because of separated flow phenomena. Early wind tunnel tests on several Orbiter configurations measured this behavior (see Ref. 3). This analysis indicates that larger variations in aerothermal heating occurred on the leeward surface of the Orbiters in flight. The mean value of the leeward surfaces on OV-102 and OV-105 (λ_L=0.166) is about twice the mean of the windward surfaces (λ_L=0.076).

The mean value of the windward surface on OV-102 (λ_L=0.078) is consistent with the mean of the windward surface on OV-105 (λ_L=0.074), and the mean value of the leeward surface on OV-102 (λ_L=0.114) is less than the mean of the leeward surface on OV-105 (λ_L=0.218). All of these mean values are slightly lower than the uncertainties predicted for the first Orbiter flight (see Fig. 1).

Separated flow phenomena and a vortex that develops where the wing joins the fuselage increase variations in aerothermal heating on the Orbiter fuselage side. The mean values for the starboard (λ_L=0.255,0.205) and port (λ_L=0.249,0.191) surfaces on OV-102 and OV-105 are greater than the windward mean values and appear to confirm this behavior. Three positions (S6,P3,P5) on OV-102 affected by these flow phenomena have high temperature outliers from the STS-1, 2, 3, 4, 5 and STS-9 missions. Post-flight analysis indicated that high Reynolds number heating effects, above that which was obtainable in the developmental wind tunnel tests, was a probable cause.[11] Because of these high structure temperatures on the early flights, the RSI was modified to provide additional margin on the OV-102 OMS pods and on OMS pods that were still under construction.[12] High temperatures were not measured on OV-105, and the mean value for the OMS pods (λ_L=0.189) is significantly less than the mean for the OMS pods on OV-102 (λ_L=0.822). Further analysis of the OMS pods is required to fully understand the effects of the RSI modification.

Thermal Strength Uncertainty or Variation

As mentioned previously, the various RSI designs at each position capture many of the actual uncertainties and randomness affecting the TPS performance capability or thermal strength. Because the RSI was fabricated and installed using aerospace requirements for material specifications, manufacturing tolerances and assembly procedures, λ_S is expected to be small. Variability in the initial temperature of the structure

before re-entry is also small due to operational flight constraints.

On the OV-102 windward and leeward surfaces λ_S is remarkably uniform, and the windward mean value (λ_S=0.033) is slightly greater than the leeward mean (λ_S=0.027). Similar uniformity occurs on OV-105, where the windward mean value (λ_S=0.041) and the leeward mean (λ_S=0.040) are nearly identical. At all leeward positions on OV-105 the λ_S are about 50% greater than OV-102. This overall increase on the leeward surface may be the result of RSI modifications that occurred in the ten years between assembly of the two Orbiters.

On the OV-102 starboard and port surfaces, λ_S is less uniform and consistent. The largest discrepancy occurs on the OMS pods (S6,P5), where the starboard pod (λ_S=0.064) is almost twice the port pod (λ_S=0.037). These values are almost identical to the OMS pods on OV-105. The consistent discrepancy on the OMS pods, where the starboard side (λ_S=0.064) is always greater than the port side (λ_S=0.038), possibly indicates some type of design asymmetry.

In general, the strength uncertainty is less than the load uncertainty. The mean value of λ_S (0.037) on the windward surface is about 50% of the mean value of λ_L on the windward surface (0.076). On the leeward surface λ_S (0.034) is about 20% of λ_L (0.166), and on the starboard and port surfaces λ_S (0.042) is about 20% of λ_L (0.225). These trends indicate that it is important to implement manufacturing specifications and initial temperature constraints to insure λ_S is sufficiently less than the variations in the load environment (λ_L).

Factor of Safety

Of the many positions examined in analyzing the general trends exhibited by λ_L and λ_S, two of the most interesting are on the OMS pods (S6,P5), where the original RSI design was improved to eliminate the high structure temperatures measured on the early flights of OV-102. This improvement increased the FOS on the OMS pods from a mean value of FOS=2.59 on OV-102 to a mean of FOS=4.49 on OV-105.

On the windward surface of OV-102 the FOS are distributed around a mean value of FOS=2.36, which is very consistent with the mean of FOS=2.35 on OV-105. On the leeward surface of OV-102 the FOS are distributed around a mean value of FOS=5.29, which is slightly greater than the mean of FOS=4.83 on OV-105. The leeward mean value for OV-102 and OV-105 is about FOS=5.06. The largest discrepancy occurs above the cockpit (T8), where FOS=10.04 on OV-102 and FOS=5.79 on OV-105.

The mean values of FOS on the windward and leeward surfaces are consistent with the relationship between FOS, λ_S and λ_L in Fig. 2. On the windward surface FOS=2.35 with λ_S=0.037 and λ_L=0.076. Fig. 2 indicates that when λ_L increases, a larger FOS (moving the means (μ_S, μ_L) further apart) is required to minimize the strength-load interference region. This behavior is demonstrated on the leeward surface where FOS=5.06 with λ_S=0.034 and λ_L=0.166.

Index of Reliability

In developing components or systems to satisfy a reliability requirement, it is necessary to design for the nominal environment, and also evaluate the capability to withstand occasional, off-nominal events. The index of reliability provides a probabilistic estimate of reliability for the nominal environment. In this analysis, it provides an estimate of the thermal reliability of thirty-three RSI designs operating in the re-entry environments of the OV-102 and OV-105 missions. The effect of occasional, off-nominal events, such as surface damage from impact debris, should be assessed by a probability risk assessment of the degraded RSI performance.

As shown in Fig. 3, the index of reliability (IOR) is an adequate measure of reliability. In examining the local values of IOR on each of the Orbiters it is important to recognize that uncertainty exists in these estimates, particularly at positions with low values of r^2 and temperature outliers.

On OV-102, the mean values of IOR on the windward (IOR=12.0), starboard (IOR=11.9) and port (IOR=11.1) surfaces are remarkably consistent. The mean IOR on the leeward surface (IOR=24.1) of OV-102 is more than twice the mean on the other surfaces, suggesting that the RSI designs on the leeward surface are overly conservative.

On OV-105 the three surfaces that are the most consistent are the windward (IOR=10.9), starboard (IOR=14.4) and leeward (IOR=13.4). The port surface on OV-105 (IOR=20.4) is about 1.8 times greater than the port surface on OV-102 (IOR=11.1).

After discarding the two outliers (24.1,20.4), a mean value of IOR=12.3 is estimated for the Orbiter RSI positions, which is equivalent to a thermal reliability greater than 'fifteen 9s' for the nominal re-entry trajectories of the missions used in this analysis.

Again, two of the most interesting positions are on the OMS pods (S6,P5). The RSI improvement increased the IOR on the OMS pods from a mean value of IOR=1.9 on OV-102 to a mean of IOR=11.6 on OV-105. This was a critical upgrade because the thermal reliability of IOR=1.9 is only 97.1%, significantly less than the RSI thermal reliability at other positions.

Discussion

Reliability estimates from this NDLI analysis represent the thermal reliability of the RSI at thirty-three positions, and are not an estimate of the overall reliability of the entire thermal protection system installed on an Orbiter. Estimates of the overall system level reliability require a probabilistic risk assessment of the performance and interaction of the individual components in the system.[13,14] Probabilistic methods such as NDLI are only useful in estimating the reliabilities of individual components. Connecting the components together and examining the probabilistic cause and affect of their interactions is accomplished by probabilistic risk assessment techniques. In addition to assessing overall system reliability under nominal conditions, the probabilistic risk assessment is also typically used to examine the effect of anomalies or incidents that may occur infrequently yet have catastrophic effects.

Because the TPS is a thermal-structural system it is important to assess both the thermal and mechanical reliability of all the critical failure modes. This very limited study has examined only the thermal reliability of one critical failure mode (structure temperature), of just one component family (RSI), at only a few positions.

Reliability is affected by the differences between the design environment and the actual operating environment. In 1972, President Nixon directed NASA to begin development of the Space Shuttle System as the nation's primary launch vehicle and to gradually phase out the existing expendable launch vehicles. To satisfy the military requirements for launching into a polar orbit from the western test range (WTR) and landing after one orbit, the Orbiter was designed with higher crossrange capability than that required for low orbit inclination launches from the eastern test range (ETR). Thicker RSI is required to adequately insulate the structure during high orbital inclination missions and high crossrange re-entry trajectories because of the increase in total integrated heat load (see Fig. 10).[15] The TPS on OV-102 was designed for a moderate heat load as an intermediate step towards achieving this goal. One of the original goals of the OV-102 Orbiter Flight Test (OFT) program (STS-1 through STS-5) was to gradually expand the flight envelope and gather data for assessing polar orbit capability. Data on the performance of the windward RSI during the OFT program indicated that the OV-102 windward TPS has the capability for a polar orbit mission, although the heat loads exceed the design limits at some positions.

After the Challenger accident in 1986, polar orbit missions were no longer seriously considered and the Orbiter missions were constrained to re-entry trajectories at a narrower range of low inclination angles with lower heat loads. Most of the structure temperatures used in this analysis were measured under these conditions. Because both the mean value (μ_L) and variation (λ_L) are lower than the values that would be expected if polar orbit missions were flown, the estimates of RSI thermal reliability in this analysis are higher than the original design requirements. Further analysis of the actual heat loads corresponding to the data in Table 1 and 2 is required for accurate comparison to the design requirements.

The OFT flights also indicated that three factors (see Fig. 11) combined to decrease structure temperatures on the windward surface.[16,17] The laminar heating was lower because of non-catalytic surface effects. The turbulent heating occurred later in the trajectory because of delayed transition from laminar to turbulent flow. Additional atmospheric cooling occurred below Mach 2.5 when the vent doors were opened. These factors contribute to reducing μ_L in Table 1 and 2, and as a result, have increased the RSI thermal reliability on the windward surface.

The RSI thermal reliabilities are calculated from structure temperatures measured on as many as twenty-seven missions flown over more than twenty years. During this time the RSI is subject to many environmental factors during each mission cycle that may or may not affect performance. The post-flight reports (see Ref. 7 and 8) document the more severe effects of debris impacts, contamination, seal leakage, thermal shorts, etc. that require maintenance, which ranges from simple in-situ repairs to component replacement. Any maintenance that affects the structure temperature is captured by the load parameters (μ_L,λ_L) in the NDLI analysis. For example, the adhesive used to bond the RSI to the exterior wall of the structure has also been applied to the interior wall where high structure temperatures have been measured. Increasing the effective thermal capacitance of the structure will decrease the structure temperature and the mean value

(μ_L). As a result, the RSI thermal reliability is increased.

At positions that have only required minimum refurbishment, the original RSI material has experienced the nominal aging process associated with reusable launch vehicle operations (ascent, on-orbit, re-entry, and refurbishment). Any significant changes in the original RSI material that affect the structure temperature are captured by the load parameters (μ_L,λ_L) in the NDLI analysis. As a hypothetical example; if repeated waterproofing caused a gradual increase in thermal conductivity and a slight increase in structure temperature over many missions, then the mean value (μ_L) and variation (λ_L) would also increase. As a result, RSI thermal reliability is decreased.

In addition to the effects of the trajectory, maintenance and material properties on reliability, the initial temperature (T_I) is also an important factor. Before re-entry is initiated the temperature of the structure is required to be less than a maximum limit that depends on position and total heat load.[18] Under normal circumstances the Orbiter is pointed and rotated to satisfy these requirements. If circumstances occur where the structure temperature equals the design limit temperature before re-entry (T_I=T_D), then there is no margin of safety and the structure temperature has a 100% probability of exceeding T_D. In this case, 0% reliability occurs regardless of the maximum structure temperature (T_A) observed during re-entry. This behavior suggests that T_I affects thermal strength (μ_S,λ_S) more than thermal load (μ_L,λ_L).

Pre-Flight RSI Thermal Reliability

In preparing for the first launch of OV-102 in 1981, an assessment was made of the RSI design at several representative positions to establish the thermal margin for the early OFT missions.[19] In this section, NDLI is applied to calculate RSI thermal reliabilities from this published data, and the results are compared to reliabilities calculated from the flight data.

The pre-flight assessment examined the effect of uncertainties in re-entry heating and the RSI thermal response by using the temperatures at the surface and structure to define the critical failure modes. Twelve positions (see Fig. 12) on the Orbiter were selected to assess each of the characteristic heating environments. Four areas were examined: nose, centerline (C/L), leeward (Lee) and interactions (Inter.). Heating uncertainties were established from extensive wind tunnel testing and flowfield analyses that extrapolated the test database to flight. RSI thermal response uncertainties were based on limited data, parametric numerical studies of the flowfield-RSI behavior, and general engineering judgment. Critical failure occurs at conditions that cause the surface or structure temperatures to exceed their design limits.

Reference 19 first established a nominal thermal response using: an OFT trajectory, the nominal heating parameters and the nominal material properties. Next, the most important parameters were perturbed to determine the effect on the surface and structure temperatures. In assessing thermal margin, only perturbations ($+\sigma$) from the nominal conditions that increased the surface and structure temperatures were important. The high confidence required in manned space flight designs was established by a $+3\sigma$ perturbation of each parameter. Structure temperature deviations ($\Delta T_{3\sigma}$) for a $+3\sigma$ perturbation of each parameter are listed in Table 4.

Sensitivity derivatives were used to select the important parameters. The structure temperature was most sensitive to variations in: surface heating rate ($\Delta T_{q,3\sigma}$), time of boundary layer transition from laminar to turbulent ($\Delta T_{t,3\sigma}$), thermal conductivity of the RSI ($\Delta T_{k,3\sigma}$), effective thermal capacitance of the structure ($\Delta T_{c,3\sigma}$) and the initial temperature of the RSI to substructure inner bondline ($\Delta T_{To,3\sigma}$).

The maximum temperature of the structure at the $+3\sigma$ conditions ($T_{max,3\sigma}$) was estimated by adding the root-sum-square (RSS) of the $\Delta T_{3\sigma}$ values in Table 4 to the maximum temperature of the structure at nominal conditions (T_{max}). Thermal margin (T_{margin}) is the difference between T_D and $T_{max,3\sigma}$, where a negative margin indicated failure. All of the positions had positive margin except for body point 1100 on the windward centerline near the nose.

NDLI is applied to calculate the RSI thermal reliability at the positions in Table 4. The temperature deviations ($\Delta T_{1\sigma}$) for one standard deviation ($+1\sigma$) that are used to estimate the uncertainties (λ_L,λ_S) are found by dividing $\Delta T_{3\sigma}$ by three. For comparison to the Orbiter flight data, four parameters (q,t,k,c) are selected to perturb the thermal load, and one parameter (To) perturbs the thermal strength. The RSS method is used to estimate σ_L from: $\Delta T_{q,1\sigma}$, $\Delta T_{t,1\sigma}$, $\Delta T_{k,1\sigma}$, $\Delta T_{c,1\sigma}$, and σ_S from: $\Delta T_{To,1\sigma}$. RSS is a classic method for estimating σ by combining deviations from parameters that are independent and normally distributed.

The load and strength uncertainties (λ_L,λ_S) at each position are listed in Table 5 and 6. The mean values (μ_L,μ_S) are estimated from Eq. (4) and IOR is estimated from Eq. (2). The heating uncertainties in Fig. 1 are compared to λ_L in the last column of Table 5, and there is generally good agreement between these two pre-flight assessments. The largest discrepancy occurs at the shock impingement area on the wing leading edge (2510) and the body flap (224).

The NDLI parameters ($\lambda_L\lambda_S$,FOS,IOR) are shown in Fig. 12 and listed in Table 7. Because MOS is based on nominal conditions it is always greater than a T_{margin} calculated for the 3σ condition. At body point 1100 which had a negative T_{margin}, (-19.4 K), the MOS is positive (8.0 K), the FOS is slightly greater than one (1.05) and IOR=0.9. The reliability corresponding to IOR=0.9 is 81.2%, indicating an expected failure rate of 18.8%. Another position on the windward surface closer to the nose (1024) is more reliable, and has an IOR=3.7 that slightly exceeds the 3σ requirement (IOR=3) in Ref. 19. The reliability at the remaining positions is significantly greater than IOR=3.

NDLI parameters ($\lambda_L\lambda_S$,FOS,IOR) from analysis of the pre-flight assessment and the Orbiter flight data are compared in Table 8 for body points and measurements near each other. This comparison indicates that the thermal reliability (IOR) from the pre-flight assessment is consistently lower than the Orbiter results except at body point 1750, and that good agreement occurs at 1400 and 224. All of the leeward body points have lower values of IOR than the Orbiter results, with a maximum IOR near the cockpit (3150). In addition, λ_S is consistently 30% to nearly 50% lower than the Orbiter results except at T8 on OV-102. In contrast, λ_L is much less consistent but has good agreement at body point 1750 on both Orbiters, and at 4620 on OV-105. In general, the FOS are lower than the Orbiter results except at body points 1750 and 224, with good agreement at 1400 on both Orbiters. The increase in FOS along the centerline (C/L), from body point 1100 to 1750, is opposite the trend in the Orbiter results.

Because of the uncertainties and variations in these parameters it is also useful to compare mean values in addition to comparing discrete positions. The mean value for all of the pre-flight positions (IOR=7.8) is less than the mean estimated from the flight data (IOR=12.3). The discrepancy may be caused by the difference between the nominal OFT trajectory used in the pre-flight assessment and the actual trajectories flown. A more aggressive trajectory that increases the total heat load on the RSI will reduce the MOS, FOS and IOR.

Reliability Based Design

This study has demonstrated that NDLI may be effectively applied to perform thermal reliability analysis of RSI designs from both flight data and a pre-flight TPS uncertainty assessment. The most important application of NDLI may be in the design of RSI for new reusable orbital space planes. Because overly conservative designs add mass that directly subtracts from the payload capability, it is important to optimize for mass, performance and reliability. One simple approach to optimizing the RSI design uses NDLI to specify the same reliability, or IOR, at all positions on the windward, leeward, starboard and port surfaces. This can be achieved by using Eq. (2) with a constant IOR to estimate the FOS at different positions, after the uncertainties (λ_L,λ_S) are defined. An example is provided in the last column in Table 7 for a reliability of 0.999999, and indicates that an increase in FOS from 1.05 to 1.28 is required to improve the marginal design at body point 1100. Further analysis is required to understand this new approach and develop the appropriate reliability requirements.

Conclusions

The NDLI method and statistical analysis were used to determine thermal reliability of the airframe structure at thirty-three positions on two Orbiters where reusable surface insulation (RSI) is installed. The factor of safety, load uncertainty ratio, and strength uncertainty ratio are generally in good agreement or indicate consistent trends on the windward, leeward, starboard and port surfaces. To provide a more detailed comparison of the results, the reliability is represented by the index of reliability (IOR). A mean value (IOR=12.3) from the analysis of both Orbiters indicates a reliability greater than 0.999999 (IOR=4.768). The windward surface on OV-102 (IOR=12.0) and OV-105 (IOR=10.9) are in good agreement. Early flights of OV-102 experienced high structure temperatures on the OMS pods. Improved RSI designs increased the IOR on the OMS pods from a mean value of IOR=1.9 on OV-102 to a mean of IOR=11.6 on OV-105. Further analysis of the OMS pods is required to fully understand the effects of the RSI modification.

NDLI was also used to estimate thermal reliability from an assessment of TPS uncertainties that was completed shortly before the first OV-102 flight. Results from the flight data analysis and pre-flight assessment at several positions near each other are in good agreement. The

mean value from the pre-flight assessment (IOR=7.8) is less than the mean from the flight data (IOR=12.3). Body point 1100, which was identified in the pre-flight assessment as a marginal RSI design, has a thermal reliability of only 81.2% (IOR=0.9).

The parameters affecting thermal load (q,t,k,c) and strength (To) were selected for consistency with the Orbiter flight data on the existing RSI designs. Further analysis of an RSI material that is adhesively bonded to a structure is required to fully understand the effect of the aerothermal heating parameters and the RSI thermal response parameters on thermal reliability.

Reliability based design of RSI for reusable orbital space planes is a new approach to optimizing for mass, performance, and potentially cost. A simple example demonstrated that NDLI is an effective method for estimating the factors of safety that provide a constant thermal reliability of 0.999999 for twelve body points on the Orbiter. Further analysis of this approach is required to develop the appropriate reliability requirements.

Acknowledgements

Frank Jones, Lisa Koenig at NASA KSC, and Howard Goldstein, Dan Leiser at NASA ARC provided data for the paper. Jeff Umland at NASA JPL sponsored this work for the Mars Science Laboratory program.

References

[1] Scottoline, C.A., "Determination of Aerothermodynamic Environment Uncertainties With Application to Space Shuttle Vehicles," NASA TMX-2507, Vol. II, February 1972, pp.503-518.

[2] Masek, R.V., Hender, D., and Forney, J.A., "Evaluation Of Aerodynamic Heating Uncertainties For Space Shuttle," AIAA Paper 73-737, AIAA 8th Thermophysics Conference, Palm Springs, CA, July 16-18, 1973.

[3] Haney, J.W., "Orbiter Entry Heating Lessons Learned From Development Flight Test Program," NASA CP-2283, Part 2, March 8-10, 1983, pp.719-752.

[4] Rasky, D.J. Kolodziej, P., Newfield, M.E., Laub, B., and Chen, Y.K., "Assessing Factors of Safety, Margins of Safety, and Reliability of Thermal Protection Systems," AIAA-2003-4043, June, 2003.

[5] Ayyub, B.M. and McCuen, R.H., "Probability, Statistics, and Reliability for Engineers," CRC Press, 1997.

[6] "Shuttle Operational Data Book: Volume 1, Shuttle Systems Performance and Constraints Data," NSTS-08934 (Vol. 1), Revision F, August 1995, p. 3.4.1.1-2.

[7] "Mission STS-109, OV-102 Flight 27, Thermal Protection System, Post-Flight Assessment," KLO-02-004, July 2002.

[8] "Mission STS-111, OV-105 Flight 18, Thermal Protection System, Post-Flight Assessment," KLO-02-006, October 2002.

[9] https://ssveo.jsc.nasa.gov/greenbook/, March, 2003.

[10] Hahn, G.J. and Meeker, W.Q., "Statistical Intervals; A Guide For Practioners," John Wiley and Sons, New York, New York, 1991, p.66.

[11] Office Of Advanced Manned Vehicles, "Evaluation Of The Space Shuttle Orbiter Second Orbital Flight; Descent Phase," AFFTC-TR-82-1, February 1982.

[12] Cooper, R.M., "OV-102 (OFT) OMS Pod TPS Assessment," Aerospace Report No. TOR-0083(3465-21)-1, January 3,1983.

[13] Pate-Cornell, M. and Fischbeck, P.S., "Risk Management for the Tiles of the Space Shuttle," Interfaces:24:1, Jan.-Feb. 1994, pp.64-86.

[14] Fragola, J.R., Maggio, G., Frank, M.V., Gerez, L., McFadden, R.H., Collins, E.P., Ballesio, J., Appignani, P.L., and Karns, J.J., "Probabilistic Risk Assessment of the Space Shuttle, Phase 3, A study of the potential of losing the vehicle during nominal operation, volume 1," NASA-CR-197808, Feb. 1995.

[15] Harthun, M.H., Blumer, C.B., and Miller, B.A., "Orbiter Windward Surface Entry Heating: Post-Orbital Flight Test Program Update," NASA CP-2283, Part 2, March 8-10, 1983, pp.781-804.

[16] Hoey, R.G., "AFFTC Overview Of Orbiter-Re-entry Flight-Test Results," NASA CP-2283, Part 2, March 8-10, 1983, pp.1303-1316.

[17] Stewart, D.A., Rakich, J.V., and Lanfranco, M.J., "Catalytic Surface Effects On Space Shuttle Thermal Protection System During Earth Entry Of Flights STS-2 through STS-5," NASA CP-2283, Part 2, March 8-10, 1983, pp.827-845.

[18] "Shuttle Operational Data Book: Volume V, Orbiter Flight Capability Envelopes," NSTS-08934 (Vol. V), June 1993, p. 4.1-3.

[19] Goodrich, W.D., Derry, S.M., Maria, R.J., "Effects Of Aerodynamic Heating And TPS Thermal Performance Uncertainties On The Shuttle Orbiter," AIAA Paper 79-1042, AIAA 14th Thermophysics Conference, Orlando, FL, June 4-6, 1979.

ID	λ_L	λ_S	FOS	IOR	r^2, T_L	r^2, T_S	N
Windward							
B1	0.042	0.034	1.99	12.6	0.948*	0.877*	26
B2	NA	NA	NA	NA	NA	NA	NA
B3	NA	NA	NA	NA	NA	NA	NA
B4	0.060	0.034	2.73	15.8	0.938*	0.878*	27
B5	0.106	0.028	2.06	8.8	0.911	0.927*	27
B6	0.066	0.040	2.81	13.9	0.978	0.856	27
B7	0.095	0.027	1.87	8.2	0.832	0.943	27
B8	0.093	0.033	2.10	9.5	0.874	0.955	27
B9	NA	NA	NA	NA	NA	NA	NA
B10	0.057	0.036	2.04	11.2	0.914*	0.876	27
B11	0.102	0.030	3.25	15.9	0.821	0.964	27
Leeward							
T1	0.063	0.029	5.46	26.3	0.876	0.726*	14
T2	0.140	0.026	5.17	21.4	0.944	0.936	14
T3	0.084	0.030	3.81	19.6	0.924	0.920	14
T4	0.143	0.027	4.26	17.8	0.853*	0.953*	14
T5	0.134	0.027	4.45	19.2	0.799*	0.833*	14
T6	0.111	0.029	3.95	18.4	0.983	0.982	14
T7	0.161	0.031	5.20	18.4	0.941	0.939	14
T8	0.080	0.015	10.04	52.1	0.792	0.937	14
Starboard							
S1	0.059	0.055	2.71	10.6	0.927	0.917*	27
S2	NA	NA	NA	NA	NA	NA	NA
S3	0.113	0.028	3.76	17.9	0.939	0.822*	15
S4	0.137	0.062	5.26	12.0	0.964	0.765*	27
S5	0.106	0.039	4.64	17.3	0.898*	0.683*	27
S6	0.862	0.064	2.67	1.9	0.635*	0.962	27
Port							
P1	0.053	0.053	2.66	11.1	0.973	0.842	27
P2	0.045	0.050	3.19	13.1	0.973	0.843	26
P3	0.397	0.053	2.90	4.5	0.646*	0.862*	27
P4	0.080	0.036	4.95	20.1	0.979	0.873	27
P5	0.781	0.037	2.51	1.9	0.622*	0.954*	27
P6	0.136	0.043	5.00	15.7	0.913	0.902	27
P7	NA	NA	NA	NA	NA	NA	NA
P8	NA	NA	NA	NA	NA	NA	NA

*Temperature outlier

Table 1: Non-dimensional parameters calculated from OV-102 structure temperature measurements.

ID	λ_L	λ_S	FOS	IOR	r^2, T_L	r^2, T_S	N
Windward							
B1	0.052	0.040	1.93	10.0	0.857	0.955	18
B2	0.050	0.042	2.18	11.3	0.841	0.929	12
B3	0.071	0.043	2.75	12.6	0.898	0.918*	10
B4	0.087	0.042	2.77	12.2	0.875	0.973*	18
B5	0.087	0.028	2.04	10.0	0.722*	0.964*	18
B6	0.079	0.037	2.76	13.6	0.947	0.925	18
B7	0.089	0.033	1.99	8.9	0.827	0.883*	18
B8	0.095	0.038	2.45	11.0	0.784*	0.851*	18
B9	0.069	0.058	2.08	7.7	0.780*	0.953	10
B10	0.070	0.051	2.15	8.9	0.931	0.975	16
B11	0.062	0.041	2.76	13.7	0.825*	0.912	18
Leeward							
T1	0.140	0.041	5.24	16.6	0.891*	0.750*	16
T2	0.173	0.039	4.76	14.9	0.959	0.960	16
T3	0.318	0.042	4.89	10.3	0.811*	0.970*	16
T4	0.190	0.044	3.99	11.6	0.962	0.965	15
T5	0.185	0.051	4.17	11.2	0.981	0.927	16
T6	0.340	0.036	5.12	10.6	0.734*	0.904	15
T7	0.207	0.043	4.65	12.8	0.935*	0.963	16
T8	0.187	0.028	5.79	19.3	0.815*	0.920*	16
Starboard							
S1	0.057	0.048	2.82	12.4	0.965	0.757	18
S2	0.051	0.040	2.92	14.9	0.978	0.943*	18
S3	0.066	0.027	4.10	24.2	0.858	0.925	18
S4	0.464	0.042	7.40	11.5	0.888	0.931	18
S5	0.417	0.030	6.95	12.7	0.828*	0.953	18
S6	0.174	0.064	4.63	10.6	0.922	0.952	18
Port							
P1	0.043	0.037	2.96	16.6	0.952	0.845*	18
P2	0.053	0.038	3.43	17.1	0.906	0.936*	18
P3	0.100	0.022	4.23	23.6	0.759*	0.982	18
P4	0.416	0.024	6.95	13.3	0.822*	0.866*	18
P5	0.203	0.039	4.34	12.6	0.949*	0.952*	18
P6	0.471	0.035	6.89	11.1	0.831*	0.907*	18
P7	0.070	0.015	7.27	48.2	0.939	0.775*	10
P8	0.170	0.023	5.36	20.9	0.767	0.914*	10

*Temperature outlier

Table 2: Non-dimensional parameters calculated from OV-105 structure temperature measurements.

Position	Parameter	OV	λ_L	λ_S	FOS	IOR
Windward	Minimum	102	0.042	0.027	1.87	8.2
		105	0.050	0.028	1.93	7.7
	Maximum	102	0.106	0.040	3.25	15.9
		105	0.095	0.058	2.77	13.7
	Median	102	0.079	0.033	2.08	11.9
		105	0.071	0.041	2.18	11.0
	Mean (μ)	102	0.078	0.033	2.36	12.0
		105	0.074	0.041	2.35	10.9
	Variation (σ/μ)	102	0.313	0.137	0.21	0.3
		105	0.206	0.197	0.15	0.2
Leeward	Minimum	102	0.063	0.015	3.81	17.8
		105	0.140	0.028	3.99	10.3
	Maximum	102	0.161	0.031	10.04	52.1
		105	0.340	0.051	5.79	19.3
	Median	102	0.122	0.028	4.81	19.4
		105	0.189	0.041	4.83	12.2
	Mean (μ)	102	0.114	0.027	5.29	24.1
		105	0.218	0.040	4.83	13.4
	Variation (σ/μ)	102	0.310	0.186	0.38	0.5
		105	0.329	0.161	0.12	0.2
Starboard	Minimum	102	0.059	0.028	2.67	1.9
		105	0.051	0.027	2.82	10.6
	Maximum	102	0.862	0.064	5.26	17.9
		105	0.464	0.064	7.40	24.2
	Median	102	0.113	0.055	3.76	12.0
		105	0.120	0.041	4.37	12.6
	Mean (μ)	102	0.255	0.050	3.81	11.9
		105	0.205	0.042	4.80	14.4
	Variation (σ/μ)	102	1.332	0.317	0.30	0.5
		105	0.921	0.321	0.41	0.4
Port	Minimum	102	0.045	0.036	2.51	1.9
		105	0.043	0.015	2.96	11.1
	Maximum	102	0.781	0.053	5.00	20.1
		105	0.471	0.039	7.27	48.2
	Median	102	0.108	0.047	3.04	12.1
		105	0.135	0.029	4.85	16.9
	Mean (μ)	102	0.249	0.045	3.53	11.1
		105	0.191	0.029	5.18	20.4
	Variation (σ/μ)	102	1.173	0.167	0.32	0.6
		105	0.872	0.317	0.33	0.6

Table 3: Comparison between OV-102 and OV-105 non-dimensional parameters.

ID	$\Delta T_{q,3\sigma}$	$\Delta T_{t,3\sigma}$	$\Delta T_{k,3\sigma}$	$\Delta T_{c,3\sigma}$	$\Delta T_{Tq,3\sigma}$	T_{max}	$T_{max,3\sigma}$	T_{margin}
	K (°F)	K (°F)	K (°F)	K (°F)	K (°F)	K (°F)	K (°F)	K (°F)
Nose								
1020	17.8 (32)	5.6 (10)	11.1 (20)	4.4 (8)	9.4 (17)	402.6 (265)	426.5 (308)	23.3 (42)
1024	17.8 (32)	5.6 (10)	11.1 (20)	4.4 (8)	9.4 (17)	420.4 (297)	444.3 (340)	5.6 (10)
C/L								
1100	19.4 (35)	11.1 (20)	11.1 (20)	4.4 (8)	9.4 (17)	442.0 (336)	469.3 (385)	-19.4 (-35)
1400	7.2 (13)	11.1 (20)	11.1 (20)	4.4 (8)	9.4 (17)	369.3 (205)	389.3 (241)	60.6 (109)
1750	6.1 (11)	17.2 (31)	11.1 (20)	4.4 (8)	9.4 (17)	355.4 (180)	379.3 (223)	70.6 (127)
Lee								
3104	26.1 (47)	17.2 (31)	11.1 (20)	4.4 (8)	9.4 (17)	373.2 (212)	408.2 (275)	41.7 (75)
3150	21.1 (38)	17.2 (31)	11.1 (20)	4.4 (8)	9.4 (17)	327.6 (130)	358.7 (186)	91.1 (164)
3500	26.1 (47)	17.2 (31)	11.1 (20)	4.4 (8)	9.4 (17)	352.6 (175)	387.6 (238)	62.2 (112)
4620	26.1 (47)	17.2 (31)	11.1 (20)	4.4 (8)	9.4 (17)	344.3 (160)	379.3 (223)	70.6 (127)
Inter.								
2168	28.9 (52)	17.2 (31)	11.1 (20)	4.4 (8)	9.4 (17)	338.7 (150)	375.4 (216)	74.4 (134)
2510	23.3 (42)	17.2 (31)	11.1 (20)	4.4 (8)	9.4 (17)	402.6 (265)	434.8 (323)	15.0 (27)
224	20.0 (36)	17.2 (31)	11.1 (20)	4.4 (8)	9.4 (17)	346.5 (164)	377.0 (219)	72.8 (131)

Table 4: Structure temperature uncertainties (3σ values) and margins for an OFT-type trajectory (Ref. 19).

ID	$\Delta T_{q,1\sigma}$	$\Delta T_{t,1\sigma}$	$\Delta T_{k,1\sigma}$	$\Delta T_{c,1\sigma}$	RSS, σ_L	T_A	T_I	μ_L	λ_L Ref. 19	λ_L, Ref. 3
	K	K	K	K	K	K	K	K		
Nose										
1020	5.93	1.85	3.70	1.48	7.38	402.6	283.2	119.4	0.062	
1024	5.93	1.85	3.70	1.48	7.38	420.4	283.2	137.2	0.054	
C/L										
1100	6.48	3.70	3.70	1.48	8.46	442.0	283.2	158.9	0.053	0.12 to 0.23
1400	2.41	3.70	3.70	1.48	5.95	369.3	283.2	86.1	0.069	0.12 to 0.23
1750	2.04	5.74	3.70	1.48	7.28	355.4	283.2	72.2	0.101	0.12 to 0.23
Lee										
3104	8.70	5.74	3.70	1.48	11.16	373.2	283.2	90.0	0.124	0.10
3150	7.04	5.74	3.70	1.48	9.92	327.6	283.2	44.4	0.223	0.26
3500	8.70	5.74	3.70	1.48	11.16	352.6	283.2	69.4	0.161	
4620	8.70	5.74	3.70	1.48	11.16	344.3	283.2	61.1	0.183	0.12
Inter.										
2168	9.63	5.74	3.70	1.48	11.90	338.7	283.2	55.6	0.214	0.15 to 0.23
2510	7.78	5.74	3.70	1.48	10.46	402.6	283.2	119.4	0.088	0.15 to 1.01
224	6.67	5.74	3.70	1.48	9.66	346.5	283.2	63.3	0.153	0.41

Table 5: Load parameters from NDLI analysis of Ref. 19 data and a comparison to Ref. 3 data.

ID	$\Delta T_{T0,1\sigma}$	RSS, σ_S	T_D	T_I	μ_S	λ_S
	K	K	K	K	K	
Nose						
1020	3.15	3.15	450	283.2	166.9	0.019
1024	3.15	3.15	450	283.2	166.9	0.019
C/L						
1100	3.15	3.15	450	283.2	166.9	0.019
1400	3.15	3.15	450	283.2	166.9	0.019
1750	3.15	3.15	450	283.2	166.9	0.019
Lee						
3104	3.15	3.15	450	283.2	166.9	0.019
3150	3.15	3.15	450	283.2	166.9	0.019
3500	3.15	3.15	450	283.2	166.9	0.019
4620	3.15	3.15	450	283.2	166.9	0.019
Inter.						
2168	3.15	3.15	450	283.2	166.9	0.019
2510	3.15	3.15	450	283.2	166.9	0.019
224	3.15	3.15	450	283.2	166.9	0.019

Table 6: Strength parameters from NDLI analysis of Ref. 19 data.

ID	μ_L	λ_L	μ_S	λ_S	MOS	FOS	IOR	FOS*
	K		K		K			
Nose								
1020	119.4	0.062	166.9	0.019	47.5	1.40	5.9	1.32
1024	137.2	0.054	166.9	0.019	29.7	1.22	3.7	1.28
C/L								
1100	158.9	0.053	166.9	0.019	8.0	1.05	0.9	1.28
1400	86.1	0.069	166.9	0.019	80.8	1.94	12.0	1.35
1750	72.2	0.101	166.9	0.019	94.7	2.31	11.9	1.50
Lee								
3104	90.0	0.124	166.9	0.019	76.9	1.85	6.6	1.61
3150	44.4	0.223	166.9	0.019	122.5	3.76	11.8	2.08
3500	69.4	0.161	166.9	0.019	97.5	2.40	8.4	1.78
4620	61.1	0.183	166.9	0.019	105.8	2.73	9.1	1.89
Inter.								
2168	55.6	0.214	166.9	0.019	111.3	3.00	9.0	2.04
2510	119.4	0.088	166.9	0.019	47.5	1.40	4.3	1.44
224	63.3	0.153	166.9	0.019	103.6	2.64	10.2	1.75

*Factor of safety required for a reliability of 0.999 999 (IOR=4.768)

Table 7: Index of reliability from NDLI analysis of Ref. 19 data.

Ref. 19					OV-102					OV-105				
ID	λ_L	λ_S	FOS	IOR	ID	λ_L	λ_S	FOS	IOR	ID	λ_L	λ_S	FOS	IOR
Nose														
1020	0.062	0.019	1.40	5.9										
1024	0.054	0.019	1.22	3.7										
C/L														
1100	0.053	0.019	1.05	0.9	B11	0.102	0.030	3.25	15.9	B11	0.062	0.041	2.76	13.7
1400	0.069	0.019	1.94	12.0	B12*	0.042	0.034	1.99	12.6	B12*	0.051	0.041	2.06	10.6
1750	0.101	0.019	2.31	11.9	B7	0.095	0.027	1.87	8.2	B7	0.089	0.033	1.99	8.9
Lee														
3104	0.124	0.019	1.85	6.6	P1	0.053	0.053	2.66	11.1	P1	0.043	0.037	2.96	16.6
3150	0.223	0.019	3.76	11.8	T8	0.080	0.015	10.04	52.1	T8	0.187	0.028	5.79	19.3
3500	0.161	0.019	2.40	8.4	T27*	0.124	0.029	4.53	19.4	T27*	0.259	0.040	4.86	12.2
4620	0.183	0.019	2.73	9.1	T4	0.143	0.027	4.26	17.8	T4	0.190	0.044	3.99	11.6
Inter.														
2168	0.214	0.019	3.00	9.0										
2510	0.088	0.019	1.40	4.3										
224	0.153	0.019	2.64	10.2	B5	0.106	0.028	2.06	8.8	B5	0.087	0.028	2.04	10.0

*B12 = mean value of B1,B2
*T27 = mean value of T2,T3,T6,T7

Table 8: Comparing NDLI parameters at common positions in the pre-flight TPS uncertainty assessment (Ref. 19), and the flight data of OV-102 and OV-105.

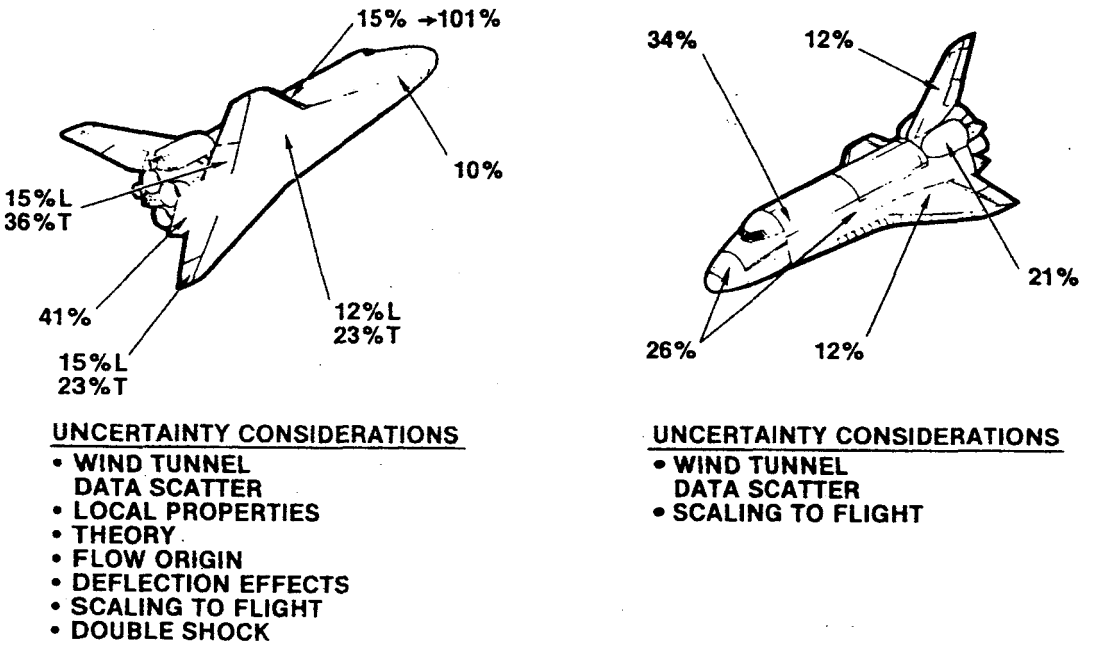

Figure 1: Heating uncertainties for assessment of the first Orbiter flight (from Ref. 3).

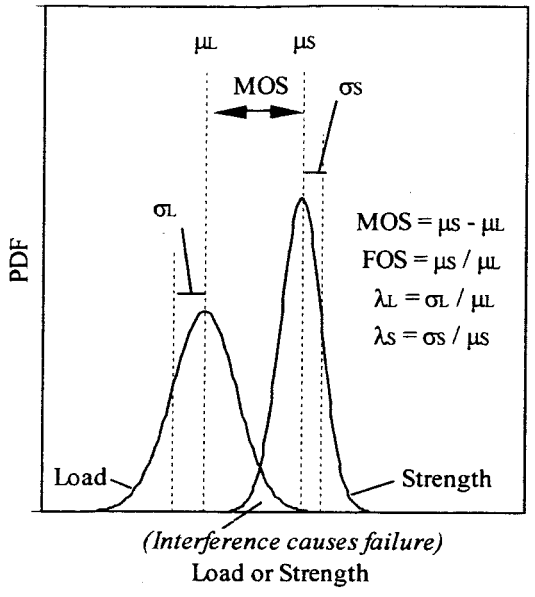

Figure 2: Examples of normal probability distribution functions for strength and load.

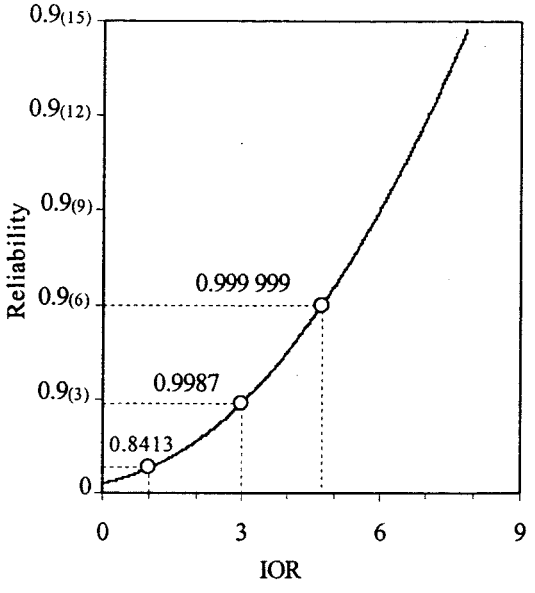

Figure 3: Relationship between the index of reliability (IOR) and reliability.

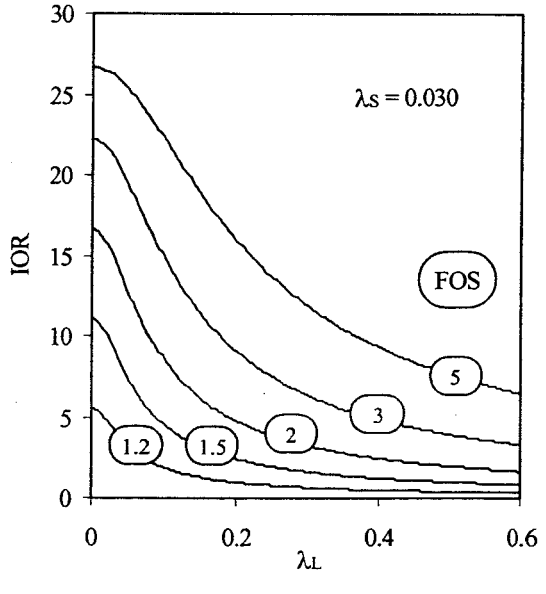

Figure 4: Effect of load uncertainty (λ_L) and factor of safety (FOS) on the index of reliability (IOR).

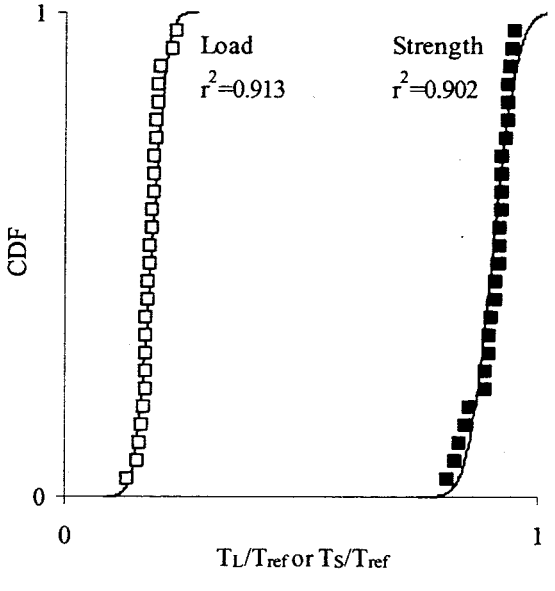

Figure 5: Correlation of normal probability distributions to OV-102 measurements of load (T_L) and strength (T_S) temperatures at position P6.

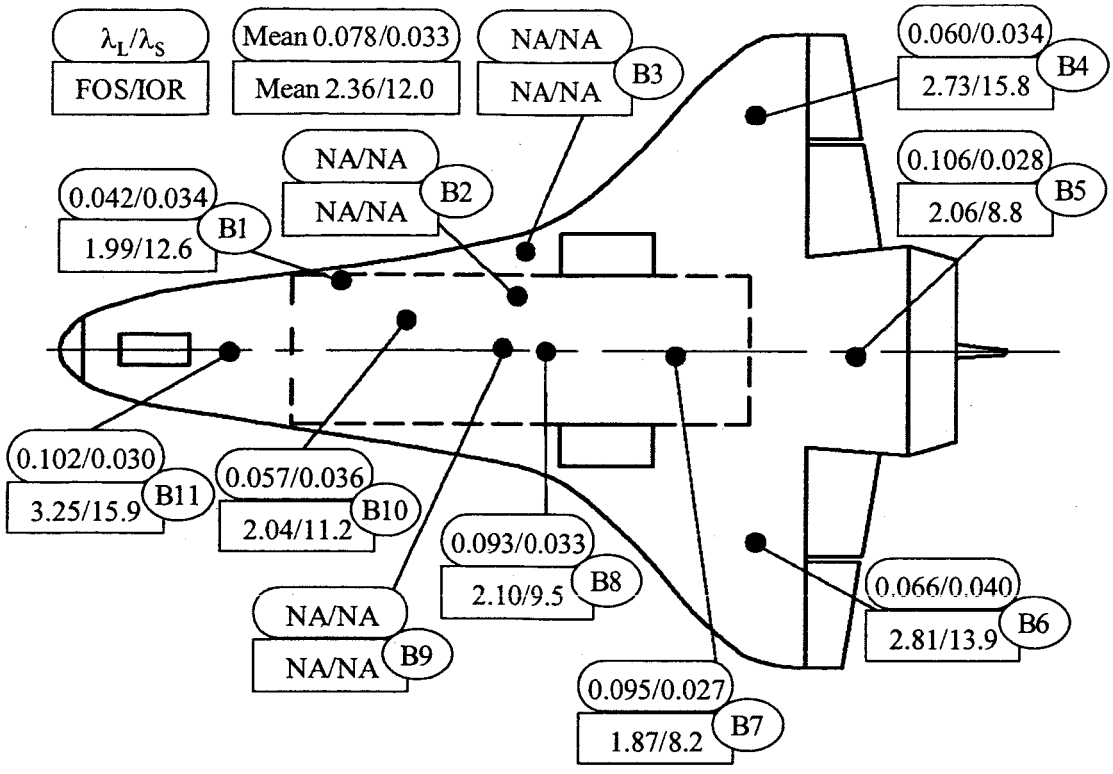

Figure 6a. Results from NDLI analysis on windward surface of OV-102.

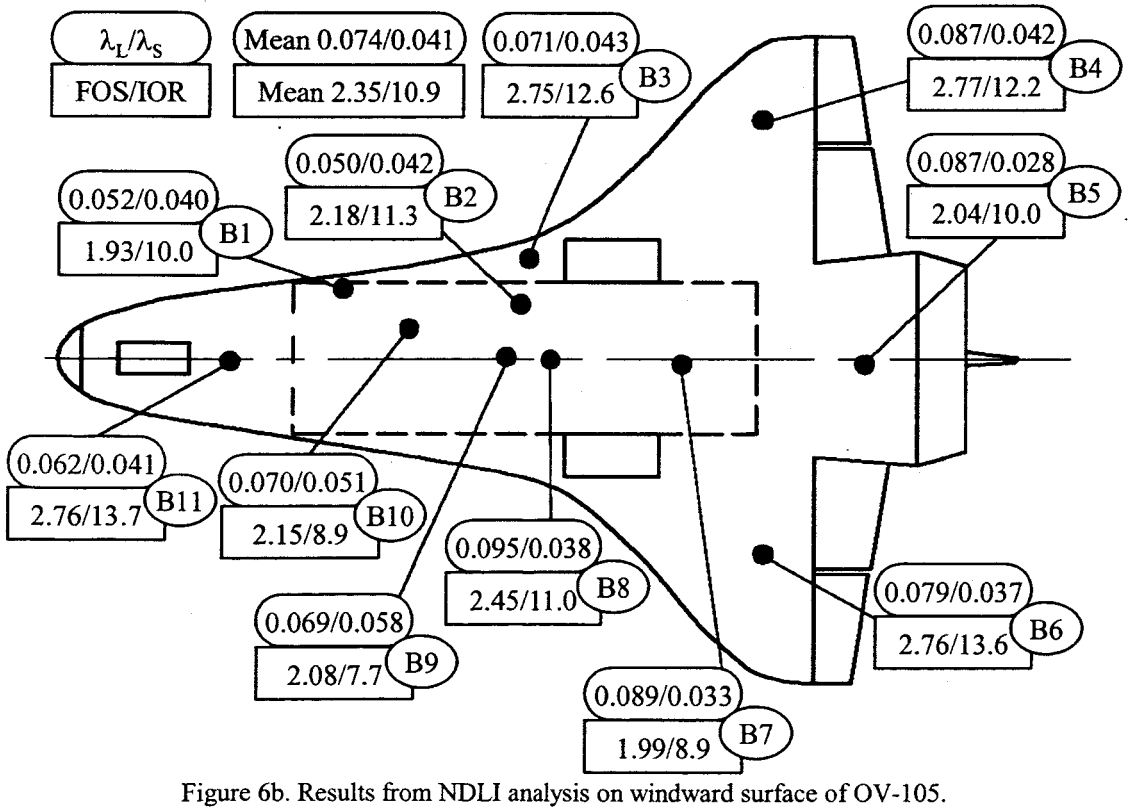

Figure 6b. Results from NDLI analysis on windward surface of OV-105.

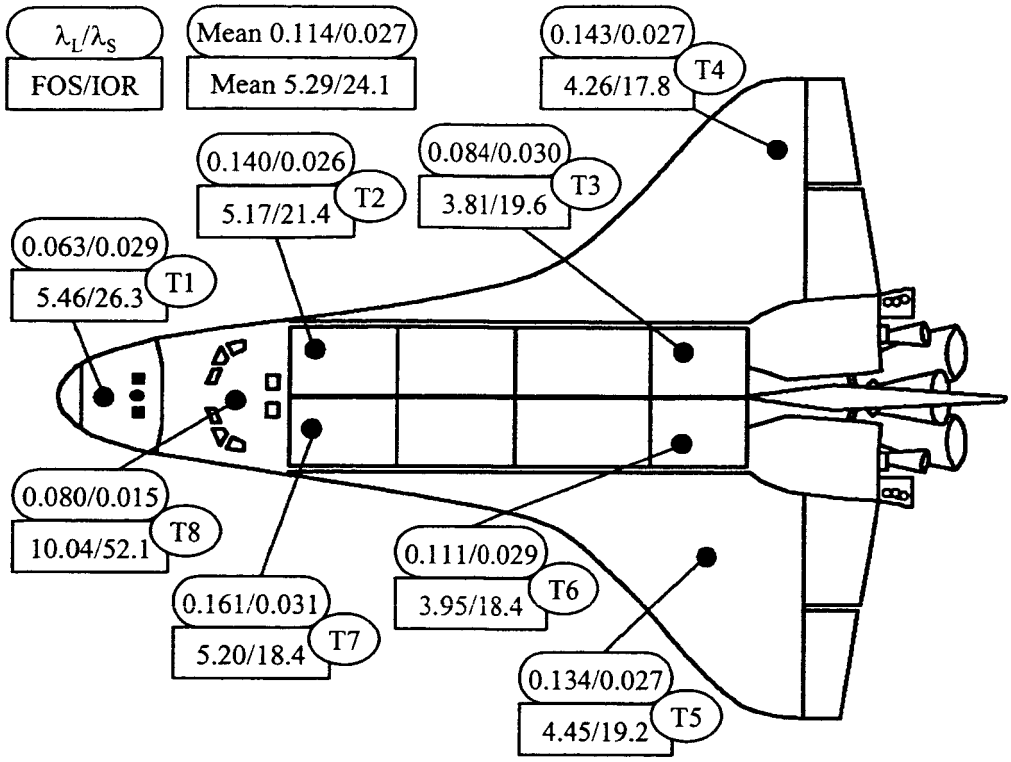

Figure 7a. Results from NDLI analysis on leeward surface of OV-102.

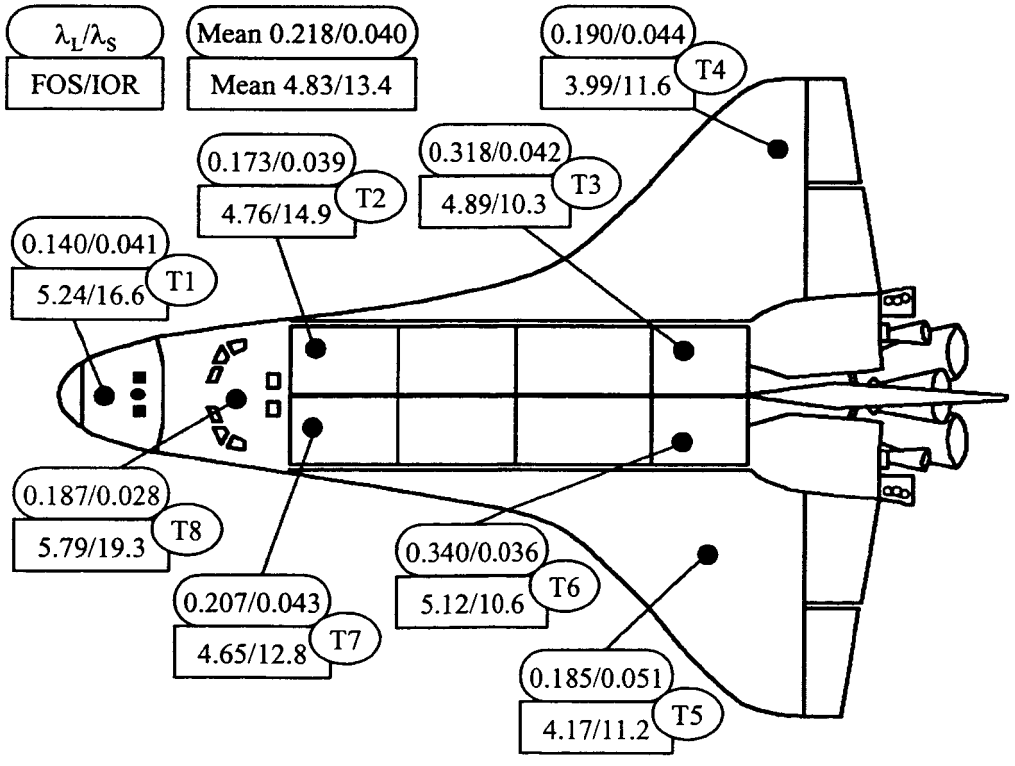

Figure 7b. Results from NDLI analysis on leeward surface of OV-105.

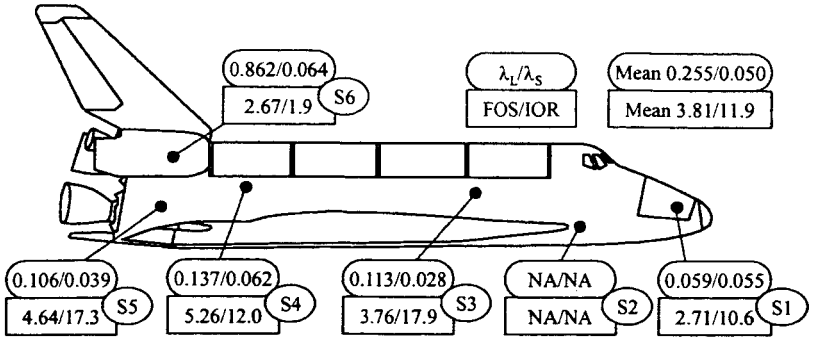

Figure 8a. Results from NDLI analysis on starboard surface of OV-102.

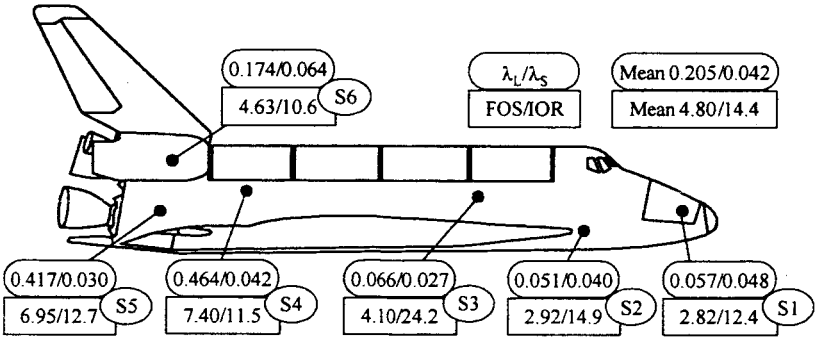

Figure 8b. Results from NDLI analysis on starboard surface of OV-105.

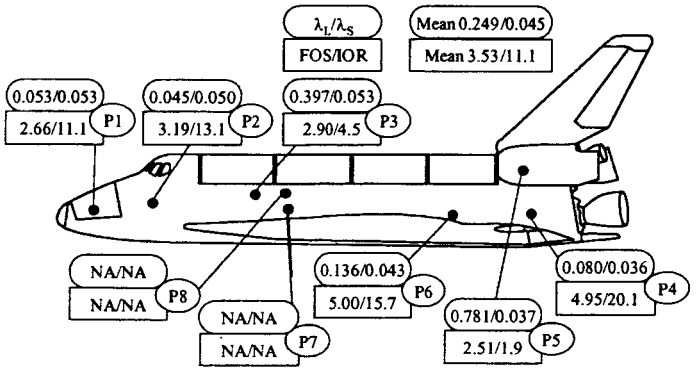

Figure 9a. Results from NDLI analysis on port surface of OV-102.

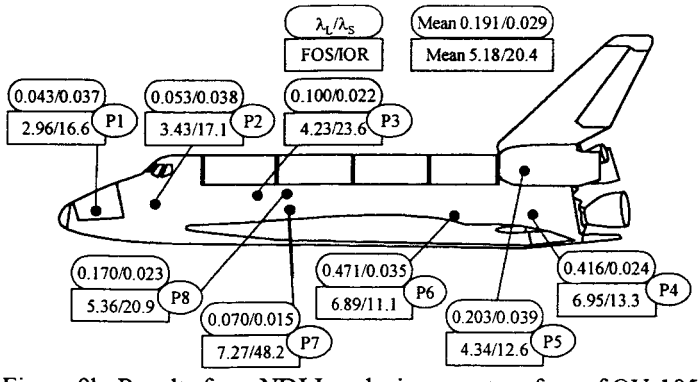

Figure 9b. Results from NDLI analysis on port surface of OV-105

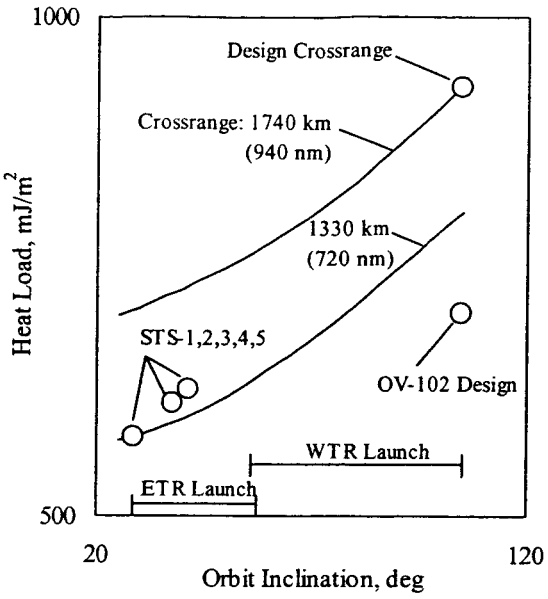

Figure 10: Heat load variation with orbit inclination and crossrange.

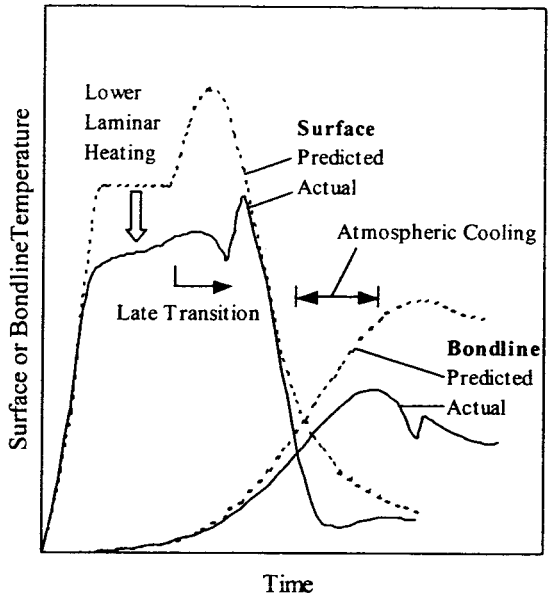

Figure 11: Decrease in actual bondline (structure) temperatures caused by lower laminar heating, late transition and atmospheric cooling.

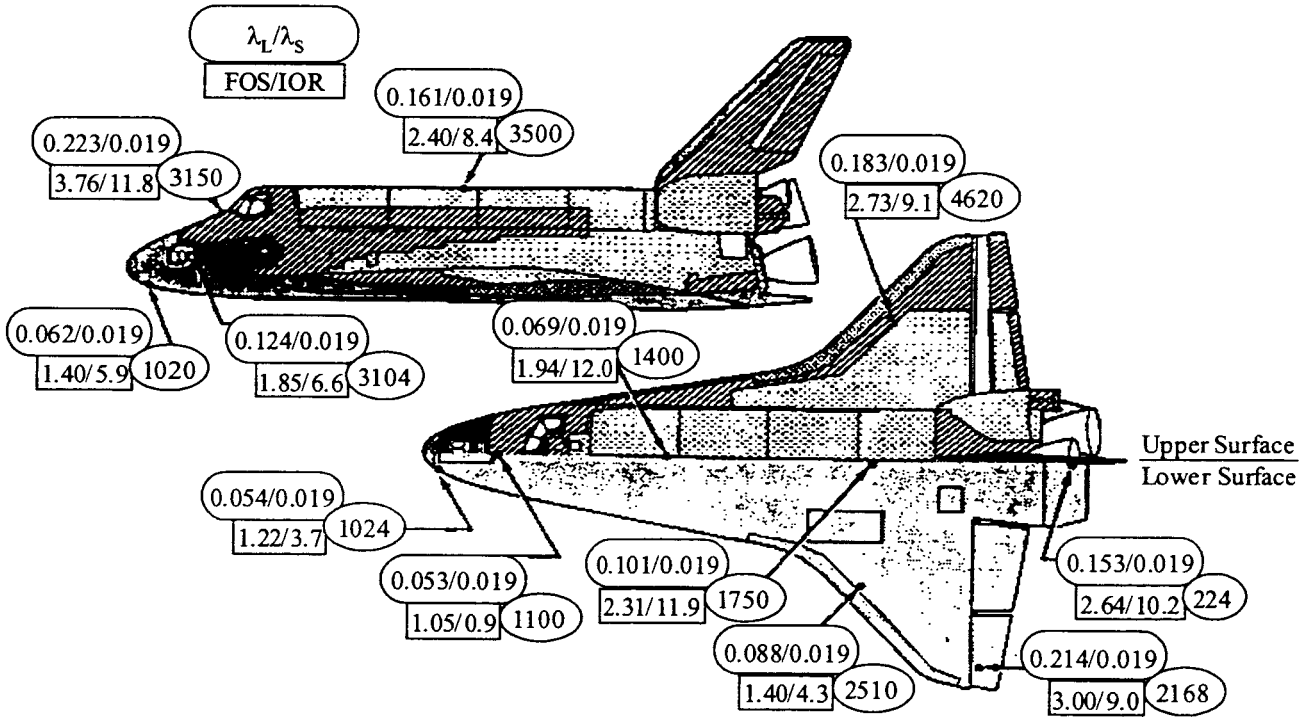

Figure 12. Results from NDLI analysis of pre-flight uncertainty assessment data (Ref. 19).